Towards Bright and Fast $Lu_3Al_5O_{12}$:Ce,Mg Optical Ceramics Scintillators

Shuping Liu ,Jiri A. Mares, Xiqi Feng, Anna Vedda, Mauro Fasoli, Yun Shi, Huamin Kou, Alena Beitlerova, Lexiang Wu, Carmelo D'Ambrosio, Yubai Pan, Martin Nikl

Abstract

The recent advent of Lu3Al5O12:Ce optical ceramics marks a turning point in scintillator material technology. Because of their lower preparation temperature, brightness, and robustness such materials can now compete with single crystals. Their further scintillation efficiency optimization includes the thorough control of the defects responsible for optical and scintillation losses. The choice of sintering agent appears critical to achieve both high optical transparency and scintillation performance. In this work, the optical investigations coupled with X-ray absorption near-edge spectroscopy evidence the beneficial role of MgO sintering agent. Mg2+ co-dopants in ceramics drive the partial conversion of Ce3+ to Ce4+. The Ce4+ center, however, does not impair the scintillation performance due to its capability to positively influence the scintillation process. The importance of simultaneous application of such co-doping and annealing treatment is also demonstrated. With 0.3 at% Mg, our ceramics display a light yield of ≈25000 photons/MeV with short 1 μs shaping time, a relative fast component intensity as high as 60%, and very low afterglow. Such performances are better than those of the isostructural single crystals ever reported. We discuss the role of co-doping and annealing in the scintillation mechanism that make such combined treatments a positive strategy for material engineering.

1 Introduction

Scintillator materials have been playing a major role in many applications where the detection of ionizing radiation is needed. Within the last two decades, a number of excellent scintillators based on Ce^{3+} and Pr^{3+}-doped materials, together with truly novel nanoscintillators, nanocomposites, and phase-separated material systems, have been discovered and studied in depth.1-8 This high R&D activity in the scintillator field was triggered by the pressing needs of modern medical imaging and radiotherapy, of high-energy physics, homeland security, and environmental applications. Among them, Ce-doped $Lu_3Al_5O_{12}$ (LuAG:Ce) aluminum garnets have attracted much attention because of their relatively high density of 6.73 g cm^{-3}, 5d – 4f electric dipole allowed radiative transition of Ce^{3+} with emission at around 500–550 nm, fast scintillation response of about 60 ns, and high theoretical light yield (LY) value of 60000 photons/MeV.9, 10 It was found that LuAG:Ce single crystal containing 0.55 at% Ce^{3+} ions prepared by Bridgman technique is a highly competitive scintillator displaying a LY of about 26000 photons/MeV with a shaping time of 1.5 μs, close to that of Lu_2SiO_5:Ce (LSO:Ce).11 Based on the understanding of defect chemistry, an effective bandgap engineering approach was successfully applied to the LuAG system. Multicomponent garnets, featuring a balanced admixture of Gd and Ga cations in the Lu-based garnet structure, form a new family of materials with an amazingly high light yield up to 58000 photons/MeV, a value exceeding that of the best $Lu_{2-x}Y_xSiO_5$:Ce (LYSO:Ce) materials by about 40%.12-15 Therefore, oxides based on garnet structure are presently considered as competitive candidates for advanced scintillation applications.

However, the low segregation coefficient of Ce^{3+} ions in the LuAG lattice is detrimental for the growth of homogeneously doped large LuAG:Ce single crystals, especially for high Ce^{3+} concentrations (Ce^{3+} > 0.2

at%).16 It was also noticed that Lu_{Al} antisite defects (AD) can severely deteriorate the scintillation characteristics of LuAG:Ce single crystals by acting as shallow traps, thus delaying the energy transport to the Ce^{3+} emission centers.17 Therefore, extensive research has recently been aimed at the preparation of ceramic analogues, which are characterized by lower preparation temperatures, more uniform doping, and lower cost. One point to consider is that during the fabrication process of transparent ceramics, sintering agents are widely used to improve the optical transparency and great success has been achieved in Nd:YAG laser ceramics.18, 19 However, differently from the laser process, which involves localized excitations, carrier migration to the luminescent centers during the scintillation process could be severely delayed by point defects induced by sintering agents. As a result, the commonly used simultaneous introduction of sintering agents like $(C_2H_5O)_4Si$ (tetraethyl ortho-silicate, TEOS) and MgO in laser ceramics induces a transparency improvement accompanied unfortunately by a deterioration of the scintillation properties.20 Therefore, strategies different from those employed for laser ceramics should be investigated and developed to simultaneously improve the optical quality and performance of ceramic scintillators. In a recent preliminary study, we showed that air-annealing treatment combined with divalent ions co-doping has a positive influence on the scintillation of aluminum garnet ceramics. A LY of about 21900 photons/MeV was obtained for Mg^{2+} co-doped LuAG:Ce ceramics with a short shaping time of 1 μs, which is 22% higher than that of the latest generation of LuAG:Ce single crystal pixels with the same thickness (2 mm).21 This result is in accordance with previous findings obtained for LSO:Ce crystals, showing that Me^{2+} co-doping (Me = Ca, Mg) significantly increases the LY and shortens the scintillation decay time.22, 23

The presence of Ce^{4+} centers in the LSO:Ce^{3+},Me^{2+} structure due to local charge compensation following Me^{2+} co-doping was clearly be identified by its charge transfer (CT) absorption located in the UV and considered responsible for the improved scintillation performance displayed by the material.24, 25 Participation of Ce^{4+} in the scintillation process was suggested to occur also in sol–gel silica glasses.26, 27 In this case the presence of Ce^{4+} is related to the oxidizing atmosphere during the glass synthesis rather than to a co-doping effect.

We have recently proposed that the stable Ce^{4+} ions in LuAG:Ce,Mg ceramics can positively participate in the scintillation process.21 Similarly to what occurs in the other materials mentioned above,24 these Ce^{4+} ions, although not luminescent under direct photoluminescence excitation, act as precursors of temporary Ce^{3+} centers that are created during irradiation with ionizing radiation and contribute to fast scintillation working in parallel with stable Ce^{3+} centers. The concentration of Ce^{4+} ions participating as precursors of temporary Ce^{3+} centers in the luminescence process is determined by the concentration of Mg^{2+} co-dopant and by the conditions of post-preparation annealing treatments.

In this paper, we investigate in detail the role of Mg^{2+} co-doping by considering both as-sintered and air-annealed LuAG:Ce,Mg ceramics with Mg^{2+} concentrations varying from 0.1 to 0.6 at% and Ce^{3+} concentration of 0.3 at%. Extensive optical investigations coupled with X-ray absorption near-edge spectroscopy (XANES) allow to evidence the tuning of Ce^{3+}/Ce^{4+} ratios by the Mg^{2+} admixture and the quantitative relationship between the Mg^{2+} and Ce^{4+} ions concentrations. The presence of point defects, related charge traps, and their dependence upon Mg co-doping is also studied. Discussion on the results of material optimizations includes comparison with commercially available LuAG:Ce and bismuth germanate (BGO) single crystals.

2 Results and Discussion

2.1 Evidence of Ce4+ – Optical Absorption and XANES

Figure 1 shows the absorption spectra of both as-sintered and air-annealed LuAG:Ce,Mg ceramics. The absorption bands at about 447 and 347 nm are related to the Ce^{3+} 4f →$5d_1$ and $5d_2$ transitions, respectively. The absorption pattern below 300 nm is composite due to the overlap of the higher 4f → 5d Ce^{3+} absorption bands and various intrinsic and trace-impurity (Fe^{3+}, Yb^{2+}) related absorptions.28, 29 The presence of the Ce^{4+} charge transfer (CT) absorption peaking at about 240 nm, which increases with increasing Mg concentration, also adds to the absorption band below 300 nm, similarly to what has been observed for LuAG:Ce,Mg and $Gd_3Al_2Ga_3O_{12}$:Ce,Mg (GGAG:Ce,Mg) single crystals.30, 31 Before annealing, this additional CT absorption band is only observable for the highest Mg concentration (0.6%). It becomes much stronger after the air-annealing process as it can be observed for all the LuAG:Ce,Mg ceramics in most of which absorption saturation occurs (Figure 1b). The constant absorption observed in the visible region for high Mg^{2+} co-doped ceramics is due to light-scattering processes.

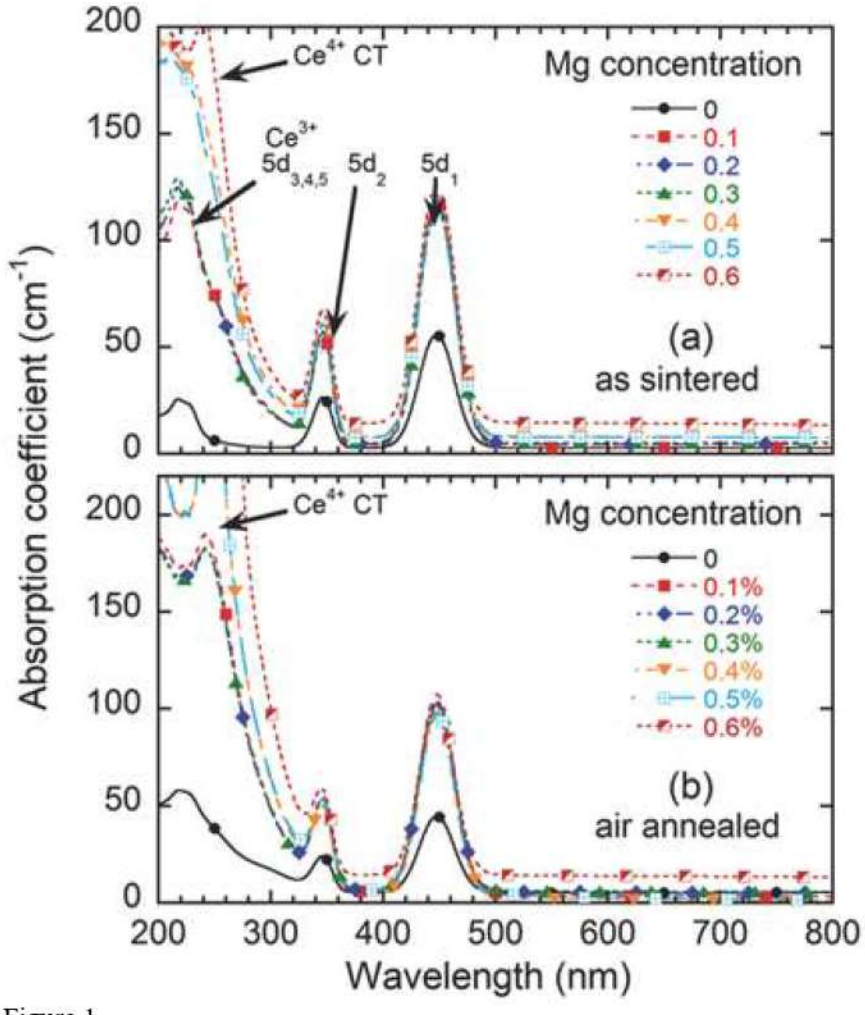

Figure 1

Optical absorption spectra of a) as-sintered and b) air-annealed LuAG:0.3% Ce ceramics with different Mg co-dopant concentrations.

XANES measurements were also performed to confirm the presence of Ce^{4+} ions and the effect of the Mg^{2+} concentration with respect to that of Ce^{3+}. The Ce L_{III}-edge XANES spectra of as-sintered LuAG:Ce,Mg ceramics are shown in Figure 2, where they are also compared with standard trivalent and tetravalent Ce compounds. The XANES spectra of all our ceramics showed the evident features characteristic of both Ce^{3+} and Ce^{4+} ions. With increasing Mg co-dopant concentration, the Ce^{4+} absorption peak at 5737 eV clearly increases. A similar trend was also observed in Me^{2+} (Me = Mg, Ca) co-doped LSO single crystals and $Lu_{0.8}Sc_{0.2}BO_3$:Ce polycrystalline powders.[24, 32] By using a linear combination fit method, proportions of the Ce^{3+} and Ce^{4+} contributions in the spectra have been estimated. The fitted results are reported in Table 1. In the Mg-free ceramic, the content of Ce^{4+} was about 15%. The Ce^{4+} fraction did not change significantly for Mg concentrations lower than 0.3%, but it clearly increased from 26% to 37% when the Mg concentration was increased from 0.3% to 0.6%. This result is in agreement with the optical absorption results. Moreover, it suggests that for Mg concentrations between 0.1% and 0.3%, the concentration of oxygen-related defects (O^- centers and/or oxygen vacancies) increased, rather than that of Ce^{4+} centers, to achieve overall charge compensation. The incorporation of Mg^{2+} co-dopant and the role of defects will be discussed in Section 2.4.

Table 1. Ceramic sample characteristics, Ce^{3+}/Ce^{4+} contents, LY and ER values, PL decay time, parameters of scintillation decays, and afterglow amplitudes of LuAG: 0.3 at%Ce ceramics with different Mg co-dopant concentrations. A double-exponential function $I(t) = \sum A_i \exp[-t/\tau_i]$ (i = 1, 2) was used to fit the scintillation decay curves and the relative intensity of each component $I_i = A_i\tau_i / \sum A_j\tau_j \times 100$ (i, j = 1, 2) is reported as well. "LuAG:Ce SC" is the single crystal without Mg co-doping measured for comparison

Mg concentration [at. %]	Size [mm]	Annealing	Ce^{3+} cont. [rel.%]	Ce^{4+} cont. [rel.%]	LY [ph/MeV]	ER [%]	PL decay [ns]	τ_1 [ns]/I_1 [%]	τ_2 [ns]/I_2 [%]	Afterglow at 4 ms [%]/400 ms [%]
LuAG:Ce SC	Ø10×1	Yes	-	-	16390	8.1	-	70/34	1700/66	1.3/0.1
0	Ø15×1	Yes	-	-	14760	9.6	58	69/41	1116/59	6.8/0.3
		No	85	15	9094	8.2	59	65/46	888/54	18.9/3.1
0.1	Ø15×0.5	Yes	-	-	23920	6.0	58	65/59	886/41	0.6/0.02

Mg concentration [at. %]	Size [mm]	Annealing	Ce^{3+} cont. [rel.%]	Ce^{4+} cont. [rel.%]	LY [ph/MeV]	ER [%]	PL decay [ns]	τ_1 [ns]/I_1 [%]	τ_2 [ns]/I_2 [%]	Afterglow at 4 ms [%]/400 ms [%]
0.2	Ø15×0.5	Yes	-	-	24550	6.7	59	64/57	1212/43	0.6/0.02
		No	75	25	10590	16.5	58	58/46	1310/54	3.3/0.16
0.3	Ø15×0.5	Yes	-	-	25070	4.9	59	64/58	981/42	0.8/0.02
		No	74	26	11690	15.6	58	58/46	1490/54	3.3/0.11
0.4	Ø15×0.5	Yes	-	-	22990	7.5	59	65/58	1064/42	0.8/0.02
		No	71	30	9370	18.6	59	57/45	1240/55	3.3/0.14
0.5	Ø15×0.5	Yes	-	-	23220	7.6	58	66/55	1135/45	1.0/0.02
0.6	Ø15×0.5	Yes	-	-	19450	8.3	59	62/60	799/40	0.6/0.01
		No	63	37	6000	-	58	54/47	1003/53	2.6/0.12

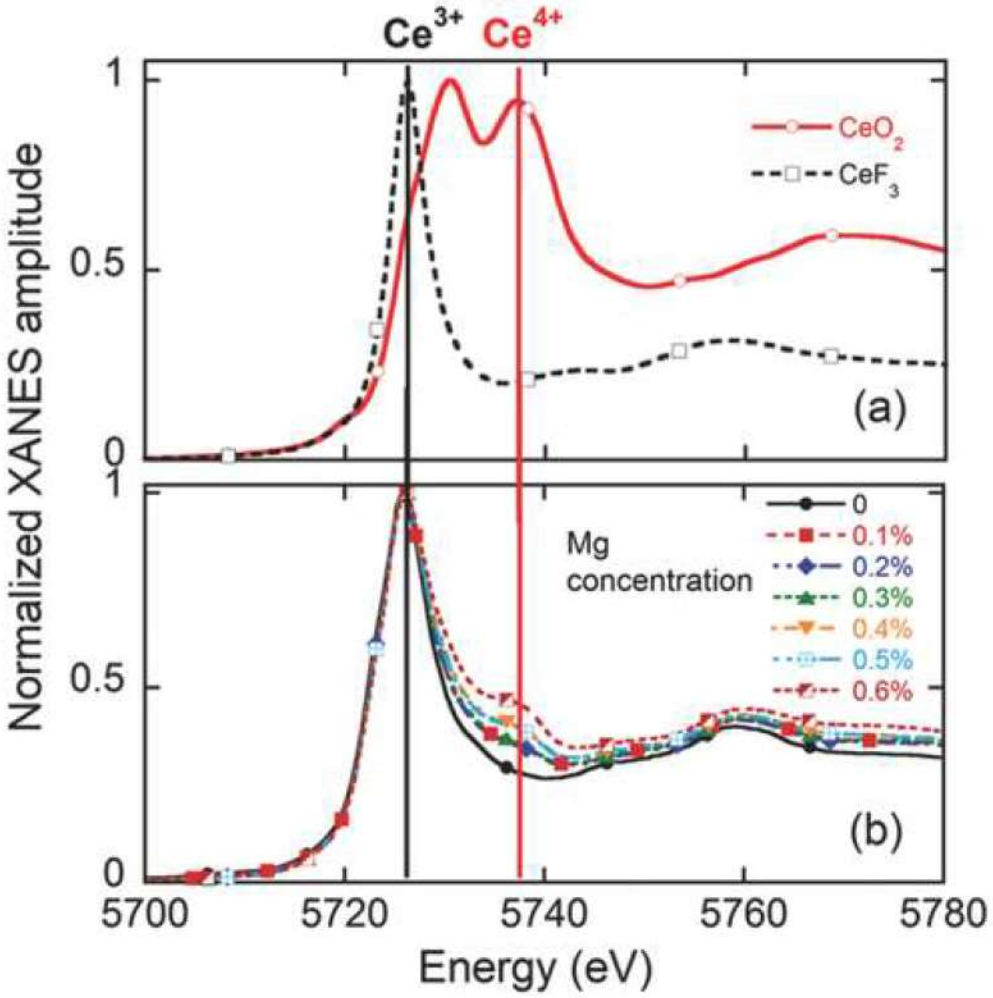

Figure 2
Room-temperature XANES measurements on the cerium L_{III}-edge (5723 eV) spectral region of a) Ce^{3+} and Ce^{4+} reference samples and b) as-sintered LuAG:0.3 at%Ce ceramics with different Mg co-dopant concentrations.

2.2 Luminescence, Scintillation, and Timing Properties

The radioluminescence (RL) spectra of some selected ceramics are displayed in Figure 3a. The $5d_1 - 4f$ ($^2F_{7/2, 5/2}$ doublet) transition of Ce^{3+} peaking at 520 nm was observed in all cases. Moreover, the Lu_{Al} antisite related luminescence could be detected in the UV region. It was very strong in the LuAG:Ce single crystal, weaker in ceramics without Mg, and almost undetectable after Mg co-doping, as shown in the inset of Figure 3a. This improvement is due both to the lower fabrication temperature of the ceramics and to the positive effect of Mg co-doping. The RL intensities depended on the Mg concentration as well as on the annealing conditions. Figure 3b shows the composition-dependent emission intensities (spectrum integrals in the 440–740 nm region related to Ce^{3+} emission). As has also previously been evidenced,21, 33 air-annealing treatment significantly improves the RL intensity because of the elimination of oxygen vacancies produced during the vacuum-sintering process. On the other hand, the RL intensity was reduced after Mg co-doping. In fact, Mg is an aliovalent impurity that can increase the concentration of some point defects, like oxygen vacancies and O^- centers, which trap carriers during irradiation. However, RL is a steady-state measurement whereas for scintillation applications the most important quantity is the light yield, i.e. the light intensity emitted within a time window after the irradiation pulse, typically in the microsecond time scale. The effect of annealing on the LY is similar to that on RL, whereas the effect of

Mg on this quantity is partially opposite to that on the RL results, as shown in Figure 3b,c. Such difference can be explained by the influence of both the annealing conditions and the Mg concentration on the defects and their distinct role played by defects in RL and LY, as it will be discussed in Section 2.4.

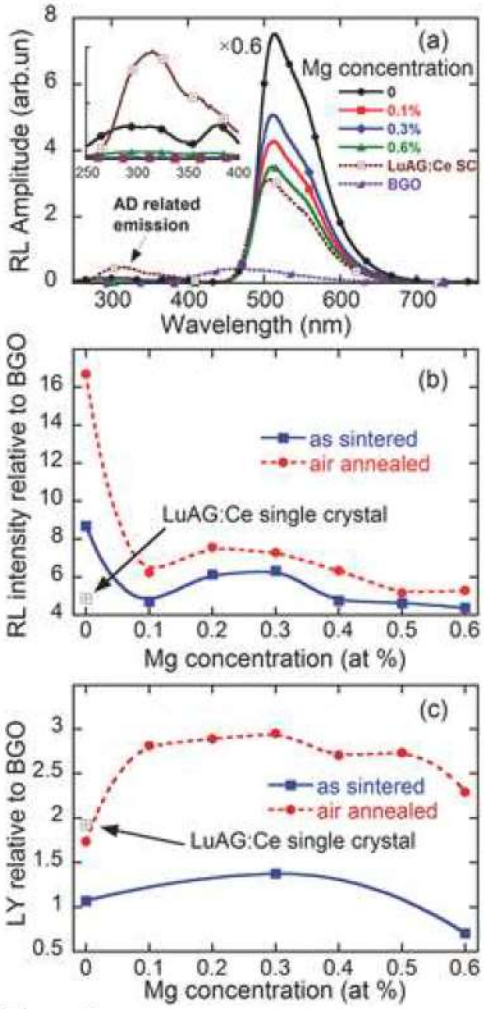

Figure 3
a) RL spectra of air-annealed LuAG:0.3% Ce ceramics with different Mg co-dopant concentrations, together with that of LuAG:Ce and BGO reference single crystals; b) RL intensity of LuAG:Ce,Mg ceramics versus Mg^{2+} co-doping concentrations. c) LY of LuAG:Ce,Mg ceramics versus Mg^{2+} co-doping (measured with a shaping time of 1μs). In both (b) and (c) data are normalized to BGO, the symbols are experimental data and the lines are just guides to the eye. The error bars are smaller than the data points.

In Figure 4 the absolute (panel a) and relative (panel b) LY values of LuAG:Ce,Mg ceramics (S and A in the figures denote "as-sintered" and "air-annealed", respectively) are reported as a function of shaping time from 0.5 μs to 10 μs. The values for the single crystal are also reported as a reference. The number of photoelectrons ($N_{phels}(E)$), energy resolution (ER), and non-proportionality properties of the best LuAG:Ce,Mg ceramic (with 0.3% Mg) and that of a LuAG:Ce single crystal as a function of γ-ray energy are shown in Figure S1 and Figure S2 in the Supporting Information, respectively. The LY, ER, and non-proportionality properties of the samples were substantially influenced by the Mg content and by the annealing process. Such detailed study showed that: i) the annealed 0.3% Mg ceramic displays the highest LY among all ceramic samples. In fact it reaches about 25000 photons/MeV when using a short shaping time of 1 μs, which is much higher when compared to the reference LuAG single crystal (16390 photons/MeV); ii) the LY values of the best ceramic and that of a LuAG:Ce single

crystal are comparable when using a 10 μs shaping time (28200 and 27600 photons/MeV, respectively); iii) the difference between the LY values at the shortest (0.5 μs) and the longest (10 μs) shaping time in annealed LuAG:Ce,Mg ceramics, non-annealed ones, and LuAG:Ce single crystal is around 15%, 70%, and 110%, respectively; iv) annealed LuAG:Ce,Mg ceramics exhibit better ER properties than the LuAG:Ce single crystal (about 4.9% against 8.1% at 662 keV, see Table 1); v) the single crystal exhibits a slightly better non-proportionality than that of the ceramics (around 64% against 70% at around 20 keV, respectively). Furthermore, the deep trapping defects that compete with the luminescent centers for charge-carrier capture could be permanently filled and made inactive by a pre-irradiation process. As a result of such a procedure, a significant improvement in the stability of both the RL efficiency and light yield was indeed obtained in several scintillator single crystals like $BaAl_4O_7$:Eu, YPO_4:Ce,Nd, $Lu_2Si_2O_7$:Pr, $Bi_4Ge_3O_{12}$, $Lu_{0.3}Y_{0.7}AlO_3$:Ce, and LuAG:Ce.[34-36] For LuAG:Ce, a RL increase of about 30% was noticed after an X-irradiation at 50 Gy.[36] Such a process could possibly work also for LuAG:Ce,Mg ceramics and give rise to a further improvement of their performance.

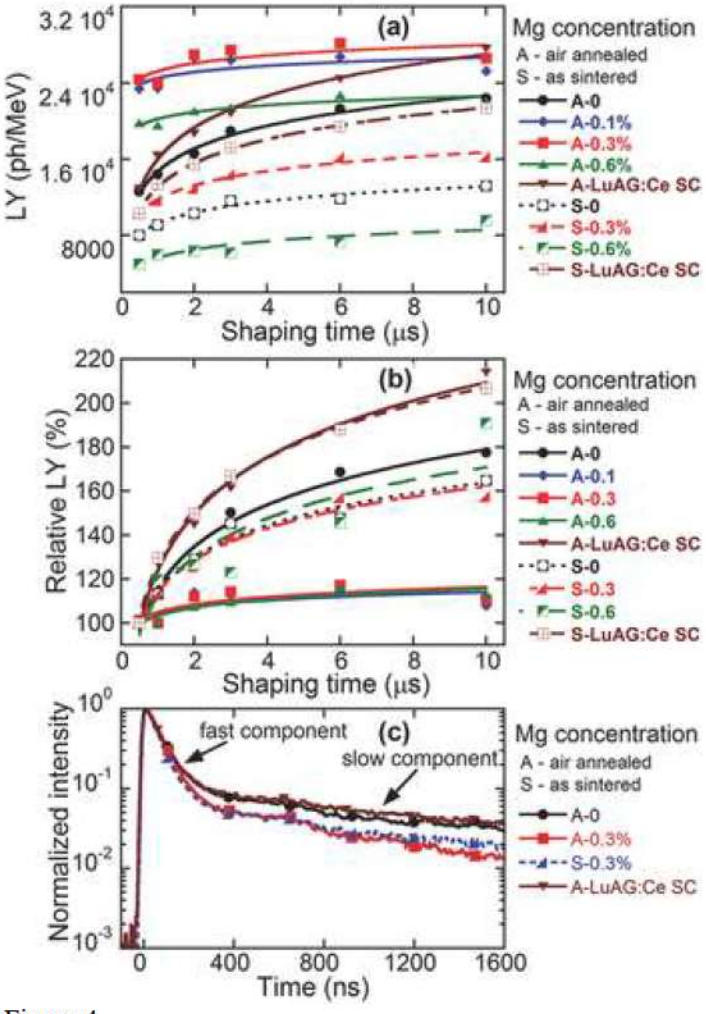

Figure 4

a) Light yield of air-annealed LuAG:0.3% Ce ceramics with different Mg co-dopant concentrations and of a LuAG:Ce single crystal as a function of shaping time in the 0.5 – 10 μs range; b) Relative light yield of samples obtained by normalizing the curves in (a) by the LY for a 0.5 μs shaping time; c) Normalized scintillation decay curves of a Mg-free LuAG:Ce ceramic, of as-sintered and annealed LuAG:Ce,Mg ceramics (0.3% Mg co-doped samples) and of a LuAG:Ce single crystal (excitation ^{22}Na, 511 keV).

Figure S3 in the Supporting Information and Figure 4c show the photoluminescence (PL) and scintillation time decays, respectively, of all samples. The results of the exponential fit of the curves are included in Table 1. Neither the Mg^{2+} concentration nor the air-annealing treatment was found to influence the PL decay time, as all the PL curves were characterized by a single exponential component with a decay time of around 60 ns. The scintillation decay curves display two components, corresponding to the prompt and delayed radiative recombination at both the stable Ce^{3+} and temporary Ce^{3+} (created after electron capture by Ce^{4+}) centers, respectively. A positive role of the combination of Mg co-doping and annealing is evidenced in this case, as the relative weight of the fast scintillation decay component is about 45% in the as-sintered ceramics and this increases up to around 60% in the Mg-rich samples after the air-annealing process.

2.3 Role of Defects—Afterglow and TSL

In Figure 5, the afterglow curves of selected ceramics and of the reference LuAG:Ce single crystal are shown together with that of BGO, which is known to possess an extremely weak afterglow.37 The relative afterglow values at 4 ms and at 400 ms after X-ray cutoff (the signal level with X-rays being "on" was normalized to 1) are displayed in Table 1. The afterglow intensity was significantly reduced by the combination of Mg^{2+} co-doping and annealing. In the annealed Mg co-doped samples, we observe that the afterglow improvement, also with respect to the single crystal value, is considerable even for the lowest 0.1% Mg^{2+} concentration, while little variations are detected for higher Mg^{2+} values.

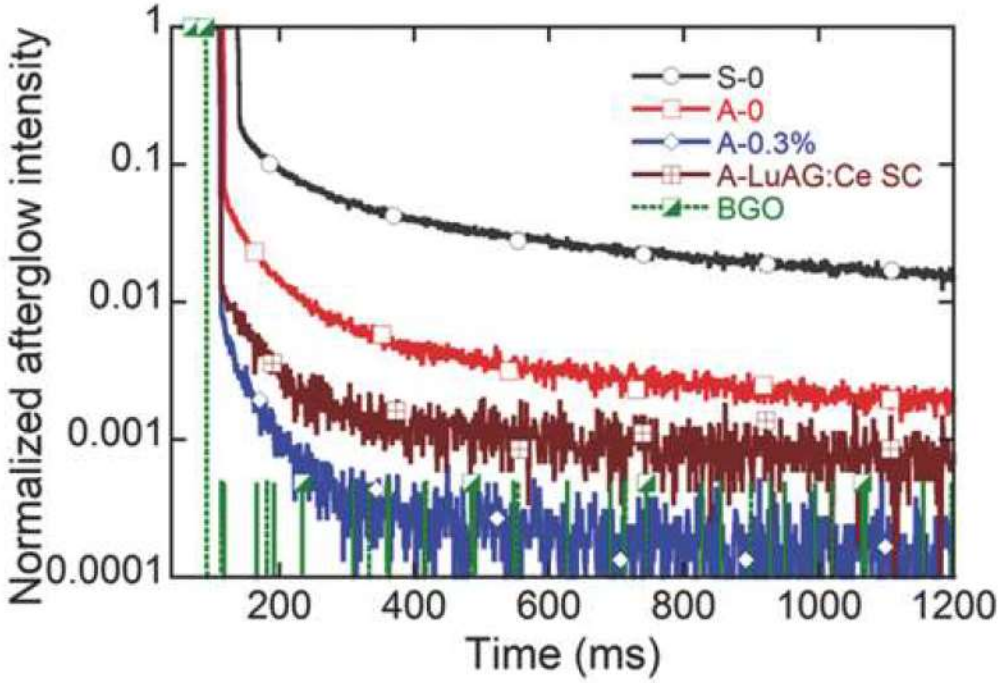

Figure 5
Spectrally unresolved afterglow time profile of LuAG:0.3% Ce ceramics with different Mg co-dopant concentrations, and of BGO and LuAG:Ce single crystals after cutting off the 40 kV X-ray excitation.

Thermally stimulated luminescence (TSL) measurements were performed with the aim to explain the role of shallow and deep traps in the RL, scintillation LY, and afterglow characteristics described above. The TSL data are reported in Figure 6a,b for the 290–800 K and 10–320 K ranges, respectively. In both graphs, the data were normalized to the RL intensity of each sample so that the TSL amplitudes depended only on the concentration of

traps in the material. The combined effect of Mg content and annealing can be discussed from comparing the data above room temperature (RT) (Figure 6a). Prior to annealing, Mg introduction causes a lowering of traps especially below 400 K. This effect is accompanied by the occurrence of additional very deep traps evidenced by the signal above 650–700 K, which are, however, reduced by the subsequent annealing. Indeed, after annealing a very strong reduction of traps concentration is noticed for all Mg concentrations and in the whole temperature interval. This result suggests the participation of oxygen vacancies in electrons traps in the TSL process. However, the signal in the highest temperature region (above approximately 400 K) was more intense after air annealing in Mg codoped samples with respect to the Mg-free ones.

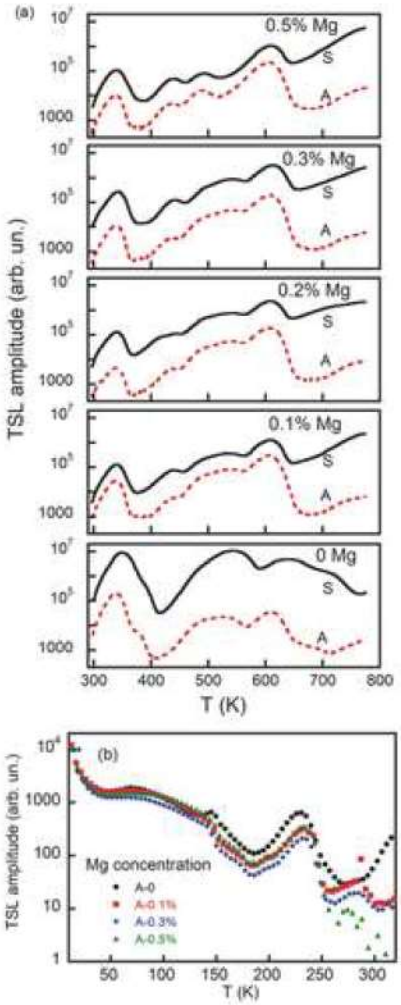

Figure 6
TSL glow curves of LuAG:0.3% Ce ceramics with different Mg co-dopant concentrations measured: a) in the 290–800 K range and b) in the 10–320 K range after X-ray irradiation at 290 and 10 K, respectively.

The TSL data at low T are presented in Figure 6b for the annealed samples. A monotonically decreasing signal (probably due to the presence of a continuous distribution of trap levels38 and/or to a-thermal tunneling recombination39) was observed, accompanied by two peaks at about 230 and 280 K and by another signal above 280 K. In accordance with the data above RT, a clear signal reduction was detected above 200 K by increasing Mg co-doping. Peaks close to RT are related to traps responsible also for afterglow. Therefore, the lowering of the amount of traps following Mg co-doping and annealing is in accordance with the afterglow improvement described above.

2.4 Incorporation of Mg2+ and Annealing—Role in Scintillation and in Defects Equilibrium

Air-annealed LuAG:Ce,Mg ceramics displayed higher LY values, better ER, and faster scintillation response than the as-sintered Mg-free ceramics and the single-crystal analogue. The defect equilibrium equations after Mg^{2+} co-doping and the air-annealing process can be described as:

$$MgO + Lu(Ce)^{\times}_{Lu(Ce)} \rightarrow Mg'_{Lu} + Ce^{\bullet}_{Lu(Ce)}\left(Ce^{4+}\right) \quad (1)$$

$$MgO + Lu(Ce)^{\times}_{Lu(Ce)} \rightarrow Mg'_{Lu} + O^{\bullet}\left(O^{-}\ \text{center}\right) \quad (2)$$

$$2\,MgO + 2\ Lu^{\times}_{Lu} \rightarrow 2\,(Mg'_{Lu}) + V_O^{\bullet\bullet} \quad (3)$$

$$V_O^{\bullet\bullet} + 2Ce^{\times}_{Lu} + O_2 \rightarrow 2\,O^{\times}_{o} + 2Ce^{\bullet}_{Lu}\left(Ce^{4+}\right) \quad (4)$$

The cross, apostrophe, and dot annotations represent the neutral, negatively (-1), and positively (+1) charged species, respectively.

During scintillation, stable Ce^{3+} centers first capture a hole from the valence band and become temporarily tetravalent; then, after capturing a free electron, they are converted into excited Ce^{3+} centers whose de-excitation gives rise to photon emission (Equations 5, 6, 7):

$$Ce^{3+} + h_v \rightarrow Ce^{4+} \quad (5)$$

$$Ce^{4+} + e_c \rightarrow \left(Ce^{3+}\right)^{*} \quad (6)$$

$$\left(Ce^{3+}\right)^{*} \rightarrow Ce^{3+} + h\nu \quad (7)$$

Here, e_c, h_v, and $(Ce^{3+})^*$ represent a conduction band (CB) electron, a valence band (VB) hole, and an excited Ce^{3+} ion, respectively. *hν* in Equation 7 refers to the emitted photon.

The charge balance required by Mg^{2+} co-doping gives rise to Ce^{4+} or O^- centers (Equations 1 and 2) and oxygen vacancies (Equation 3), whereas the air-annealing treatment mainly reduces the oxygen vacancies and increases the concentration of Ce^{4+} ions (Equation 4). In the scintillation mechanism involving stable Ce^{4+} centers, the process starts from Equation 6, followed by Equation 7 and 5 accordingly. The temporary Ce^{3+} centers need to trap a hole localized nearby after photon emission so as to be converted back to their initial Ce^{4+} state (Equation 5). As we previously discussed,40, 41 the O^- centers induced by Mg^{2+} are thus an important "hole source" for restoring the Ce^{4+} centers, which could effectively make such scintillation process more efficient. In this study, the RL and LY values suggest that for Mg^{2+} concentrations between 0.2 and 0.3%, the O^- and Ce^{4+} centers reach a balanced concentration for which the ceramic shows a maximum LY. Moreover, the Ce^{4+} centers can effectively compete with electron traps of any kind (such as AD and oxygen-vacancies related traps) for capturing electrons from the conduction band, thus causing a much lower AD-related RL intensity in the UV spectral region (see Figure 3), lower afterglow, and higher scintillation LY. The opposite trends in RL and LY dependencies on the Mg concentration displayed in Figure 3b and 3c (a decrease for RL and an increase for LY with increasing Mg concentration) are only seemingly contradictory. They can be explained with the aid of TSL measurements. Indeed the TSL data showed that, in Mg-rich annealed samples, the intensities of the peaks above 400 K, related to deep traps probably due to stable defect complexes with oxygen vacancies, were higher compared to that of the Mg-free material. These defects cause permanent trapping that lowers the steady state RL

intensity. On the other hand, the same combination of Mg co-doping and annealing caused a reduction of the peaks below 400 K, which are related to shallower traps and give rise to slow scintillation tails and afterglow. Short-time window measurements, such as LY, are possibly more sensitive to such shallow traps, therefore their reduction causes a LY increase. For the same reason, we observe an acceleration of the scintillation decay and a reduction of the afterglow in Mg co-doped ceramics.

Finally, it is worth noting that a LY decrease was detected in LuAG:Ce,Mg ceramics for Mg concentrations higher than 0.3%. For LuAG:Ce,Mg single crystals, a maximum LY of 23100 photons/MeV was observed already at very low Mg^{2+} concentrations (100 ppm, 30 times lower than the 0.3% Mg in our ceramics).30 A LY decrease for high Ca^{2+} concentrations (0.1–0.4% in the melt) has also been reported in LYSO:Ce,Ca single crystals,42, 43 but the real concentration of the Ca co-dopant in this kind of crystals was measured as low as 60 ppm.25 Even though our ceramics are more heavily doped, we expect that only a small fraction of the Mg ions diffuses into the grains and influences the scintillation, whereas the majority acts mostly as sintering aids between the grains. Moreover, phase separation may also occur for high doping concentrations. In fact, the presence of a secondary phase possibly related to the Mg compound is suggested to occur in the 0.6% Mg ceramic, as seen in the SEM image shown in Figure 7. Lattice distortion and the presence of a secondary phase were also considered to be the reasons behind a decrease in the RL efficiency and LY in LuAG:Ce,Mg ceramics when concentrations higher than 0.3% of Mg^{2+} were introduced into the ceramics.

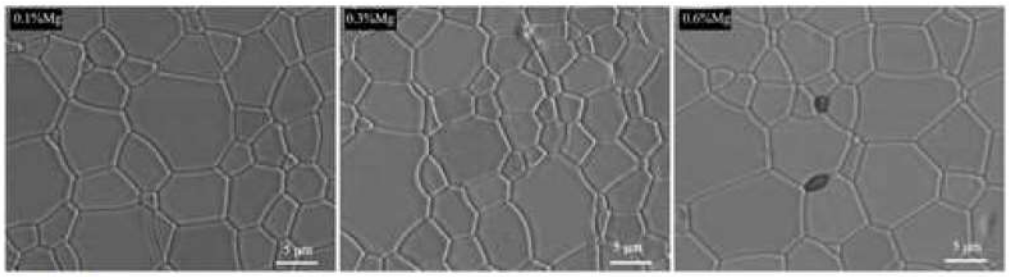

Figure 7
SEM images of mirror-polished and thermally etched surfaces of LuAG:0.3 at%Ce ceramics with different Mg co-dopant concentrations, as indicated in the panels.

3 Conclusions

Our investigation has proven that the combination of both annealing and Mg co-doping by using MgO as a sintering agent is the key to success for material optimization so that the performances of Ce-doped LuAG optical ceramics are significantly improved. By comparing the light-yield values at different shaping times and scintillation decays, we found that our ceramics displayed a more intense and faster scintillation response than commercially available isostructural single crystals. These features indicate that LuAG:Ce,Mg ceramics could be important and cost-efficient candidates in various applications, such as high-energy physics, medical imaging, and security-related techniques.

We highlighted the similarities and differences concerning the role of sintering aids in laser and scintillator ceramics. In both cases the transparency and lack of scattering were important requirements that can be fulfilled by the introduction of sintering aids. These chemical agents, like MgO employed here, were able to improve material densification, grain growth, and reduce residual porosity. For scintillators an additional and very

important role of the sintering aid consisted of modifying the point-defect concentration. Defect reduction improved the carrier-transport stage of free carriers towards the luminescent centers—a critical stage occurring only in the scintillation process—and finally this improved the scintillation performance. We have positively demonstrated this possibility for LuAG:Ce and MgO sintering aids, where defect reduction is also accompanied by tuning of the valence of the luminescent rare-earth material. These effects occur thanks to a very tight interaction of Mg with the lattice due to the real diffusion of some of the Mg ions inside the crystalline grains and their incorporation as isolated aliovalent impurities.

In the light of these considerations, future research on LuAG:Ce,Mg ceramics should be focused on the study and control of Mg diffusion into crystalline grains. Taking into account the reported radioluminescence intensities, there is ample room for further light-yield improvements. The final scope would be to tune and optimize the concentration of ions that are effectively incorporated into the LuAG lattice and contribute to the scintillation improvement, as well as the content of sintering aid, which works mostly in the interfacial regions between the grains to improve material densification. Such an investigation should also contribute to a deeper, general comprehension of the complex microscopic processes involving sintering agents, which occur during optical ceramic preparation procedures.

4 Experimental Section

$Lu_3A_5O_{12}$:0.3 at% Ce, *x* Mg (*x* = 0.1–0.6 at%) ceramics were fabricated by a solid-state reaction and vacuum-sintering method. The detailed technological route has been described in previous works.[20, 33] After sintering in vacuum, a set of LuAG:Ce,Mg ceramics was further annealed at 1450°C for 20 h in air. In order to clarify the role of the Mg co-dopant, a 0% Mg (Mg-free) LuAG:0.3 at% Ce ceramic was also included as a reference.[44] A commercial LuAG:Ce single crystal grown by the Czochralski method (Crytur Ltd., Turnov, Czech Republic), as well as a Bridgman grown BGO single crystal provided by SICCAS Corp. (Shanghai, China) were also used for comparison. All the ceramic samples were Φ15 mm plates with a thickness of 0.5–1 mm and their surfaces were optically polished. The thickness difference between the samples did not significantly influence the measurements because of the small penetration depth of the X-rays in the material. For 40 keV photons (photons with the maximum energy in the X-ray unfiltered polychromatic beam spectrum) 90% attenuation occurs within 0.5 mm.[45] The lower energy photons present in the X-ray beam were attenuated over even shorter distances.

Absorption spectra in the 200–800 nm range were measured using a Varian Cary 5000 (Varian Inc., USA) and a Shimadzu 3101PC spectrometer (Shimadzu Co., Japan). X-ray absorption near-edge structure (XANES) spectra were obtained at Beijing Synchrotron Radiation Facility (BSRF). Measurements were performed at room temperature, at the Ce L_{III}-edge (5723 eV). The uncertainty in the energy value in this measurement was ± 0.1 eV. All spectra were normalized in the same way using Athena software,[46] by which the Ce^{3+}/Ce^{4+} ratio was evaluated with an accuracy of ± 10%. Radioluminescence (RL) spectra were measured using an X-ray tube (Seifert GmbH, Germany, 40 kV) with excitation by a custom-made 5000M model Horiba Jobin Yvon fluorometer (Horiba Jobin Yvon Co., France) and equipped with a TXB-04 photon counting detector. For afterglow measurements, samples were irradiated by X-rays with the same X-ray tube (operated at 40 kV for 15 min), after which the beam was cut off and the luminescence emitted from the samples was recorded as a function of time. This set-up was also used

to measure the photoluminescence decay under a nanosecond pulse nanoLED 450-nm (Horiba Jobin Yvon Co., France) excitation source. The scintillation LY and ER were investigated using hybrid photodetectors (HPMT hybrid photomultipliers PP0470 or PP0475B manufactured by DEP, The Netherlands).47, 48 The quantum efficiency (QE) calibration of the HPMT allowed us to evaluate the LY values from $N_{phels}(E)$ photoelectron yields even in the green spectral range where QEs are below 10%; the error of the LY values was ± 5%. The $N_{phels}(E)$ values were measured from 8 to 1300 keV using different radioisotopes, such as ^{22}Na, ^{137}Cs, ^{109}Cd, ^{133}Ba, ^{57}Co, etc. The scintillation decay curves were obtained using a Hamamatsu PMT U7600 (Hamamatsu Co., Japan) and digital oscilloscope (Tektronix TDS3052, Tektronix, Inc., USA) under excitation by 511 keV photons from a ^{22}Na source. To enhance the collection of scintillation photons, a Teflon reflection tape was used to cover the samples. A good optical coupling between the samples and the photocathode window was ensured by applying Dow Corning Q2-3067 optical grease (Dow Corning Co., USA).

Thermally stimulated luminescence (TSL) measurements from 290 to 800 K were performed after X-ray irradiation at room temperature (RT) by a Machlett OEG50 X-ray tube (Machlett Labs, Inc. Stanford, USA) operated at 30 kV. A 1 K s^{-1} heating rate was adopted. The emitted light was detected by an EMI9635QB photomultiplier (Thorn. EMI Gencom, Inc., USA). Wavelength-resolved TSL measurements were also performed in the same temperature range using a home-made apparatus featuring a Jobin-Yvon Symphony CCD detector. TSL measurements in the 10–320 K range were performed after irradiation at 10 K by a Philips 2274 X-ray tube (Philips, the Netherlands) operated at 20 kV, using a homemade wavelength-resolved apparatus featuring a Jobin-Yvon Spectrum One 3000 CCD detector. In this case a 0.1 K s^{-1} heating rate was adopted. The glow curves from 10 to 320 K were obtained after integration of the wavelength-resolved data from 460 nm to 660 nm (in the range of Ce^{3+} emission).

Acknowledgements

The authors are thankful to Dr. Pengfei Yu for his help with the processing of the XANES data. The authors gratefully acknowledge the financial support from the China Scholarship Council (CSC). This work was supported by the National Science Foundation of China (No. U1332202, 61475175, 51172262), the Research Program and International Cooperation Program of Shanghai Sciences and Technology Commission Foundations (No. 13JC1405800), and the Chinese Academy of Sciences President's International Fellowship Initiative (Grant No. 2013T2G0004 and No. 2014VTB009). Partial support by the Czech Science Foundation project P204/12/0805 is gratefully acknowledged. Partial support of EC project H2020-TWINN-2015 no. 690599 (ASCIMAT) is also gratefully acknowledged.

[1] M. Nikl, A. Yoshikawa, Adv. Opt. Mater. 2015, 3, 463.

[2] I. H. Campbell, B. K. Crone, Adv. Mater. 2006, 18, 77.

[3] M. Conti, Phys. Medica 2009, 25, 1.

[4] F. P. Doty, C. A. Bauer, A. J. Skulan, P. G. Grant, M. D. Allendorf, Adv. Mater. 2009, 21, 95.

[5] N. Yasui, Y. Ohashi, T. Kobayashi, T. Den, Adv. Mater. 2012, 24, 5464.

[6] P. Lecoq, A. Annenkov, A. Gektin, M. Korzhik, C. Pedrini, Inorganic Scintillators for Detector Systems: Physical Principles and Crystal Engi-neering, Springer, Berlin, Germany 2006.

[7] O. Sidletskiy, A. Vedda, M. Fasoli, S. Neicheva, A. Gektin, Phys. Rev. Appl. 2015, 4, 024009.

[8] Y. Tang, J. Hu, A. H. Elmenoufy, X. Yang, ACS Appl. Mater. Interfaces 2015, 7, 12261.

[9] P. Dorenbos, IEEE Trans. Nucl. Sci. 2010, 57, 1162.

[10] C. R. Ronda, A. M. Srivastava, Luminescence: From Theory to Applications (Ed: C. Ronda), Wiley-VCH, Weinheim, Germany 2007, Ch. 5.

[11] C. Dujardin, C. Mancini, D. Amans, G. Ledoux, D. Abler, E. Auffray, P. Lecoq, D. Perrodin, A. Petrosyan, K. L. Ovanesyan, J. Appl. Phys. 2010, 108, 013510.

[12] M. Nikl, J. Pejchal, E. Mihokova, J. A. Mares, H. Ogino, A. Yoshikawa, T. Fukuda, A. Vedda, C. D'Ambrosio, Appl. Phys. Lett. 2006, 88, 141916.

[13] M. Fasoli, A. Vedda, M. Nikl, C. Jiang, B. Uberuaga, D. Andersson, K. McClellan, C. Stanek, Phys. Rev. B 2011, 84, 081102 (R).

[14] K. Kamada, S. Kurosawa, P. Prusa, M. Nikl, V. V. Kochurikhin, T. Endo, K. Tsutumi, H. Sato, Y. Yokota, K. Sugiyama, A. Yoshikawa, Opt. Mater. 2014, 36, 1942.

[15] N. J. Cherepy, S. A. Payne, B. W. Sturm, J. D. Kuntz, Z. M. Seeley, B. L. Rupert, R. D. Sanner, O. B. Drury, T. A. Hurst, S. E. Fisher, M. Groza, L. Matei, A. Burger, R. Hawrami, K. S. Shah, L. A. Boatner, in 2010 IEEE Nuclear Science Symp. Conf. Record (NSS/MIC), IEEE, Piscataway, NJ, USA 2010.

[16] A. G. Petrosyan, K. L. Ovanesyan, R. V. Sargsyan, G. O. Shirinyan, D. Abler, E. Auffray, P. Lecoq, C. Dujardin, C. Pedrini, J. Cryst. Growth 2010, 312, 3136.

[17] Y. Zorenko, V. Gorbenko, I. Konstankevych, A. Voloshinovskii, G. Stryganyuk, V. Mikhallin, V. Kolobanov, D. Spassky, J. Lumin. 2005, 114, 85.

[18] A. J. Stevenson, X. Li, M. A. Martinez, J. M. Anderson, D. L. Suchy, E. R. Kupp, E. C. Dickey, K. T. Mueller, G. L. Messing, J. Am. Ceram. Soc. 2011, 94, 1380.

[19] S. Jiang, T. Lu, J. Chen, Comp. Mater. Sci. 2013, 69, 261.

[20] Y. Shen, Y. Shi, X. Feng, Y. Pan, J. Li, Y. Zeng, M. Nikl, A. Krasnikov, A. Vedda, F. Moretti, E. C. Dickey, J. Am. Ceram. Soc. 2012, 95, 2130.

[21] S. Liu, X. Feng, Z. Zhou, M. Nikl, Y. Shi, Y. Pan, Phys. Status Solidi RRL 2014, 8, 105.

[22] M. A. Spurrier, P. Szupryczynski, H. Rothfuss, K. Yang, A. A. Carey, C. L. Melcher, J. Cryst. Growth 2008, 310, 2110.

[23] H. E. Rothfuss, C. L. Melcher, L. A. Eriksson, M. A. S. Koschan, IEEE Trans. Nucl. Sci. 2009, 56, 958.

[24] S. Blahuta, A. Bessiere, B. Viana, P. Dorenbos, V. Ouspenski, IEEE Trans. Nucl. Sci. 2013, 60, 3134.

[25] W. Chewpraditkul, C. Wanarak, T. Szczesniak, M. Moszynski, V. Jary, A. Beitlerova, M. Nikl, Opt. Mater. 2013, 35, 1679.

[26] M. Fasoli, A. Vedda, A. Lauria, F. Moretti, E. Rizzelli, N. Chiodini, F. Meinardi, M. Nikl, J. Non-Cryst. Solids 2009, 355, 1140.

[27] F. Moretti, A. Vedda, N. Chiodini, M. Fasoli, A. Lauria, V. Jary, R. Kucerkova, E. Mihokova, A. Nale, M. Nikl, J. Lumin. 2012, 132, 461.

[28] C. Y. Chen, G. J. Pogatshnik, Y. Chen, M. R. Kokta, Phys. Rev. B 1988, 38, 8555.

[29] Y. Shen, X. Feng, Y. Shi, A. Vedda, F. Moretti, C. Hu, S. Liu, Y. Pan, H. Kou, L. Wu, Ceram. Int. 2014, 40, 3715.

[30] M. Nikl, K. Kamada, V. Babin, J. Pejchal, K. Pilarova, E. Mihokova, A. Beitlerova, K. Bartosiewicz, S. Kurosawa, A. Yoshikawa, Cryst. Growth Des. 2014, 14, 4827.

[31] K. Kamada, M. Nikl, S. Kurosawa, A. Beitlerova, A. Nagura, Y. Shoji, J. Pejchal, Y. Ohashi, Y. Yokota, A. Yoshikawa, Opt. Mater. 2015, 41, 63.

[32] Y. Wu, G. Ren, D. Ding, G. Zhang, S. Shang, D. Sun, S. Pan, Opt. Mater. 2013, 35, 520.

[33] S. Liu, X. Feng, Y. Shi, L. Wu, J. Luo, W. Wang, Y. Pan, Opt. Mater. 2014, 36, 1973.

[34] G. Patton, F. Moretti, A. Belsky, K. Al Saghir, S. Chenu, G. Matzen, M. Allix, C. Dujardin, Phys. Chem. Chem. Phys. 2014, 16,24824.

[35] F. Moretti, G. Patton, A. Belsky, M. Fasoli, A. Vedda, M. Trevisani, M. Bettinelli, C. Dujardin, J. Phys. Chem. C 2014, 118, 9670.

[36] E. Dell'Orto, M. Fasoli, G. Ren, A. Vedda, J. Phys. Chem. C 2013, 117, 20201.

[37] G. Gévay, Prog. Cryst. Growth Charact. 1987, 15, 145.

[38] K. Brylew, W. Drozdowski, A. J. Wojtowicz, K. Kamada, A. Yoshikawa, J. Lumin. 2014, 154, 452.

[39] M. Nikl, A. Vedda, M. Fasoli, I. Fontana, V. V. Laguta, E. Mihokova, J. Pejchal, J. Rosa, K. Nejezchleb, Phys. Rev. B 2007, 76, 195121.

[40] C. Hu, S. Liu, M. Fasoli, A. Vedda, M. Nikl, X.-Q. Feng, Y.-B. Pan, Opt. Mater. 2015, 45, 252.

[41] C. Hu, S. Liu, M. Fasoli, A. Vedda, M. Nikl, X. Feng, Y. Pan, Phys. Status Solidi RRL 2015, 9, 245.

[42] M. A. Spurrier, P. Szupryczynski, K. Yang, A. A. Carey, C. L. Melcher, IEEE Trans. Nucl. Sci. 2008, 55, 1178.

[43] K. Yang, C. L. Melcher, P. D. Rack, L. A. Eriksson, IEEE Trans. Nucl. Sci. 2009, 56, 2960.

[44] S. Liu, X. Feng, J. A. Mares, V. Babin, M. Nikl, A. Beitlerova, Y. Shi, Y. Zeng, Y. Pan, C. D'Ambrosio, Y. Huang, J. Lumin. 2016, 169, 72.

[45] M. J. Berger, J. H. Hubbell, S. M. Seltzer, J. Chang, J. S. Coursey, R. Sukumar, D. S. Zucker, K. Olsen, XCOM: Photon Cross Sec- tions Database, http://www.nist.gov/pml/data/xcom/index.cfm/, accessed: September 2009.

[46] Y. Wu, J. Luo, M. Nikl, G. Ren, APL Mater. 2014, 2, 012101.

[47] J. A. Mares, A. Beitlerova, P. Prusa, K. Blazek, P. Horodysky, K. Kamada, A. Yoshikawa, C. D'Ambrosio, M. Nikl, J. Lumin. 2016, 169, 701.

[48] J. A. Mares, C. D'Ambrosio, Opt. Mater. 2007, 30, 22.